Journal of Statistical Physics, Vol. 90, Nos. 5/6, 1998

Dynamical Behavior of the Multibondic and Multicanonic Algorithm in the 3D q-State Potts Model

Malcolm S. Carroll,[1] Wolfhard Janke,[1] and Stefan Kappler[1]

Received July 18, 1997; final December 11, 1997

We investigate the dynamical behavior of the recently proposed multibondic cluster Monte Carlo algorithm in applications to the three-dimensional q-state Potts models with $q = 3$, 4, and 5 in the vicinity of their first-order phase transition points. For comparison we also report simulations with the standard multicanonical algorithm. Similar to the findings in two dimensions, we show that for the multibondic cluster algorithm the dependence of the autocorrelation time τ on the system size V is well described by the power law $\tau \propto V^{\alpha}$, and that the dynamical exponent α is consistent with the optimal random walk estimate $\alpha = 1$. For the multicanonical simulations we obtain, as expected, a larger value of $\alpha \approx 1.2$.

KEY WORDS: First-order phase transitions; Potts model; cluster representation; Monte Carlo simulations; multicanonical algorithm; multibondic algorithm; autocorrelations.

1. INTRODUCTION

Standard Monte Carlo simulations of phase transitions employing the canonical ensemble and local algorithms are severely hampered by slowing down of the pseudo-dynamics.[1] At a continuous phase transition the physical origin of *critical slowing down* is the divergence of the spatial correlation length ξ.[2,3] This implies large autocorrelation times, $\tau \propto \xi^z$, with a dynamical critical exponent $z \approx 2$, and hence greatly enhanced statistical errors, $\varepsilon \propto \sqrt{\tau}$. For d-dimensional systems of finite size $V = L^d$, ξ has to be replaced by $\min\{\xi, L\}$, such that in the immediate vicinity of the transition point $\tau \propto L^z$ for a finite system. Here the development of

[1] Institut für Physik, Johannes Gutenberg-Universität Mainz, 55099 Mainz, Germany.

0022-4715/98/0300-1277$15.00/0

non-local cluster or multigrid algorithms with dynamical critical exponents $z \ll 2$ has basically solved the problem in many applications.[4]

At a first-order phase transition[5] of models with a finite number of states per spin the correlation length stays finite at the transition point. In this case the physical origin of the problem of slowing down is due to phase coexistence. For large but finite systems in the canonical ensemble this is usually reflected by a pronounced double-peak structure of the energy (and/or magnetization) distribution, $\mathscr{P}_{\text{can}}$. The minimum region between the two peaks corresponds to mixed phase configurations which are strongly suppressed by an additional interface energy, $\mathscr{P}_{\text{can}}^{\min}/\mathscr{P}_{\text{can}}^{\max} \propto \exp(-2\sigma L^{d-1})$, where σ is the (reduced) interface tension and L^{d-1} is the cross-section of the system. To achieve thermal equilibrium and therefore the proper relative weight of the pure phases, the system must pass many times through the strongly suppressed mixed phase configurations, which results in a *super-critical slowing down* with *exponentially* divergent autocorrelation times, $\tau \propto \exp(2\sigma L^{d-1})$.[6]

One possible solution of this problem was recently discussed by Berg and Neuhaus[7-9] who proposed to perform the simulations in an auxiliary multicanonical ensemble which is related to the original canonical formulation by reweighting.[10] The reweighting factor is determined iteratively in such a way that the multicanonical energy distribution is flat between the two peaks of the canonical distribution. Then, invoking a simple random walk argument in energy space, one expects that the growth of autocorrelation times with the system size follows a much weaker power-law, $\tau \propto V^{\alpha}$, where α is the analog of the dynamical critical exponent z at a continuous transition. Actual numerical simulations of two-dimensional q-state Potts models obtain values for $\alpha \approx 1.3$,[8, 11, 12] despite the expected $\alpha = 1$ predicted by the random walk picture. These simulations have been performed with the standard local Metropolis or heat-bath algorithms, since the multicanonical reweighting procedure implicitly introduces non-local interactions such that it is not immediately obvious how to adapt, say, cluster algorithms to this situation.

In a recent letter[12] two of us proposed a solution to this problem, called the multibondic cluster algorithm. The idea is first to treat the cluster decomposition and then second to apply the reweighting concept to the bond degrees of freedom instead of to the energy. In applications to the two-dimensional q-state Potts model with $q = 7$, 10, and 20 it has been demonstrated that, with this algorithm, the optimal random walk exponent $\alpha = 1$ can be obtained.[12]

The purpose of the present note is to extend this investigation to three dimensions by performing extensive simulations with both the multibondic and multicanonical algorithms in order to make a thorough comparison.

As an application we chose the three-dimensional q-state Potts models[13] with $q=4$ and 5, which are both known to exhibit quite a strong temperature driven first-order phase transition.[14] With the multibondic algorithm our results in three dimensions are also consistent with the optimal random walk prediction, $\alpha=1$, while with the multicanonical algorithm we obtain a larger value of $\alpha\approx 1.2$. A few data are also given for the much weaker first-order phase transition of the three-dimensional 3-state Potts model which has many applications in condensed matter physics[14] and, having the symmetry of the center group of SU(3), is also of considerable interest in high-energy physics.[15] Our results clearly support the claim that for future high-precision studies of this model the multibondic algorithm is the perfect tool.

The rest of the paper is organised as follows. In Section 2 we briefly recall the model and discuss the simulation details. In Section 3 we introduce the various autocorrelation times we have measured in this study. The results are presented in Section 4, and in Section 5 we close with our conclusions and a few final comments.

2. MODEL AND SIMULATION

The q-state Potts model is defined by the canonical partition function[13, 14]

$$Z_{\text{can}}=\sum_{\{\sigma_i\}} e^{-\beta E}, \qquad E=-\sum_{\langle ij\rangle}\delta_{\sigma_i\sigma_j}, \qquad \sigma_i=1,\ldots,q \tag{1}$$

where $\beta=J/k_BT$ is the inverse temperature in natural units, the spins σ_i are located at the sites i of a simple cubic lattice of size $V=L^3$, $\langle ij\rangle$ denote nearest-neighbor pairs, and $\delta_{\sigma_i\sigma_j}$ is the standard Kronecker delta symbol. As usual we employed periodic boundary conditions in all three space directions.

In *multicanonical* simulations one simulates the auxiliary partition function

$$Z_{\text{muca}}=\sum_{\{\sigma_i\}} e^{-\beta E}e^{-f_c(E)} \tag{2}$$

where $e^{-f_c(E)}$ is an appropriate reweighting factor chosen in such a way that the multicanonical energy distribution $\mathscr{P}_{\text{muca}}(E)=\mathscr{P}_{\text{can}}(E)\,e^{-f_c(E)}$ is constant between the two peaks of the canonical energy distribution $\mathscr{P}_{\text{can}}(E)$. Even if we start without any explicit input information on the form of $\mathscr{P}_{\text{can}}(E)$, the reweighting factor $e^{-f_c(E)}$ can be constructed quite fast by an automatic iteration procedure which, at any rate, takes only a minor

Table I. Parameters of the Multicanonical (muca) and Multibondic (mubo) Simulations of the 3D q-State Potts Model[a]

q	L	β_0	N_{muca}	$\lvert E_d\rvert$	$\lvert E_o\rvert$	N_{mubo}	B_d	B_o	N
3	10	0.550500	7	1581	1821	7	686	769	100000
	18	0.550574	35	9226	10439	26	3903	4388	100000
	8	0.627939	7	665	1006	7	314	461	100000
	10	0.628215	10	1304	1920	10	612	903	100000
	12	0.628378	20	2258	3329	20	1057	1555	100000
4	14	0.628389	40	3597	5279	30	1680	2454	100000
	16	0.628534	80	5372	7855	50	2511	3692	100000
	20	0.628570	100	10536	15228	100	4920	7095	100000
	24	0.628613	100	18195	26321	100	8490	12310	40000
	30	0.628542				100	16630	23918	40000
	6	0.686965	3	238	458	7	120	224	100000
	8	0.688392	12	574	1074	21	286	532	100000
	10	0.688802	28	1118	2085	34	562	1035	100000
5	12	0.689101	45	1942	3580	55	973	1772	100000
	14	0.688676	135	3089	5672	99	1538	2816	100000
	16	0.689178	119	4620	8380	143	2303	4141	100000
	20	0.689150	229	9027	16544				34000
	20	0.689150				394	4476	8206	22000

[a] β_0 is the inverse simulation temperature, N_{muca} and N_{mubo} are the number of sweeps between measurements, $\lvert E_{o,d}\rvert$ and $B_{o,d}$ are the maxima locations of the canonical energy and bond distributions $\mathscr{P}_{\text{can}}(E)$ and $\mathscr{P}_{\text{can}}(B)$ (entering in the definition of flip times and determining the reweighting range), and N is the number of measurements.

fraction of the total simulation time. Once $e^{-f_e(E)}$ was estimated, we reweighted $\mathscr{P}_{\text{can}}(E)$ to the temperature where the two peaks of the canonical energy distribution are of equal height and determined the two peak locations E_o and E_d. Here the subscripts o and d stand short for the ordered and disordered phase, respectively. In the production runs we then used this temperature and set $e^{-f_e(E)} \propto 1/\mathscr{P}_{\text{can}}(E)$ for $E_o \leqslant E \leqslant E_d$ and $e^{-f_e(E)} = 1$ outside this range. The values for E_o and E_d as well as the inverse simulation temperature β_0 for each lattice size can be found in Table I, where information on the statistics is also given. For the update of the spins σ_i we used the heat-bath algorithm.

In *multibondic* simulations[12] one first rewrites the partition function (1) into the equivalent Fortuin–Kasteleyn representation[16] and then simulates, similar to (2), an auxiliary partition function

$$Z_{\text{mubo}} = \sum_{\{\sigma_i\}} \sum_{\{b_{ij}\}} \prod_{\langle ij\rangle} [p\,\delta_{\sigma_i\sigma_j}\delta_{b_{ij},1} + \delta_{b_{ij},0}]\, e^{-f_b(B)} \tag{3}$$

where the additional degrees of freedom $b_{ij}=0$ or 1 live on the bonds of the lattice,

$$p=\exp(\beta)-1 \tag{4}$$

and $e^{-f_b(B)}$ is the multibondic reweighting factor chosen in such a way that the multibondic *bond* distribution $\mathscr{P}_{\text{mubo}}(B)$ is constant between the two peaks of the canonical bond distribution $\mathscr{P}_{\text{can}}(B)$. Here

$$B=\sum_{\langle ij\rangle} b_{ij} \tag{5}$$

is the total number of active bonds with $b_{ij}=1$. The update of the bond variables b_{ij} and spins σ_i proceeds basically as in the standard Swendsen–Wang cluster algorithm:[17]

1. If $\sigma_i \neq \sigma_j$, set $b_{ij}=0$ as usual. If $\sigma_i=\sigma_j$, then assign new values $b_{ij}^{\text{new}}=0$ and 1 with relative probabilities $e^{-f_b(B')}$: $pe^{-f_b(B'+1)}$, where $B'=B-b_{ij}^{\text{old}}$.
2. Identify clusters of spins that are connected by "active" bonds ($b_{ij}=1$).
3. Draw a random value 1...q independently for each cluster and assign this value to all spins in a cluster.

The only difference is that, when testing whether a proposed new value for b_{ij} can be accepted, the reweighting factor $e^{-f_b(B)}$ also has to be taken into account.

By differentiating $\ln Z$ with respect to β, where Z is given as in (1) or (3) with $e^{-f_b}\equiv 1$, it is easy to see that

$$-\langle E\rangle=(1+1/p)\langle B\rangle \tag{6}$$

For temperatures below the transition temperature this implies that the peak locations E_o and B_o of the canonical energy and bond distributions are related by $-E_o\approx(1+1/p)\,B_o$. For temperatures above the transition temperature the subscript o has simply to be replaced by d. Inserting $\beta_t\approx 0.6285$ for $q=4$ ($\beta_t\approx 0.6892$ for $q=5$) in (4) we find $p\approx 0.875$ and $1+1/p\approx 2.14$ ($p\approx 0.992$ and $1+1/p\approx 2.01$ for $q=5$), which explains the factors between E_o and B_o, or E_d and B_d, in Table I.

This observation suggests that close to the first-order transition point, $\beta\approx\beta_t$, the double-peak structures of $\mathscr{P}_{\text{can}}(E)$ and $\mathscr{P}_{\text{can}}(B)$ should also look very similar when plotted versus $-E$ and $(1+1/p)\,B$, respectively. In fact,

for the two-dimensional models the two curves turned out to be almost identical.[12] A plot of the two distributions for the three-dimensional model with $q=4$ and $L=20$ as obtained in the multibondic simulation by reweighting is shown in Fig. 1(b). Here the differences turn out to be a little more pronounced than in two dimensions. This becomes more obvious when comparing directly the histograms of the multibondic simulation in Fig. 1(a). While the bond histogram is approximately flat (as it should be, of course, by construction of the multibondic weights), the energy histogram develops a small peak on the disordered side. This effect is, however, so small that the knowledge of one reweighting factor, $e^{-f_e(E)}$ or $e^{-f_b(B)}$, still allows to construct the other with sufficient accuracy.

To facilitate an easy comparison of the performance of the multibondic and multicanonical update algorithms we chose in both simulations

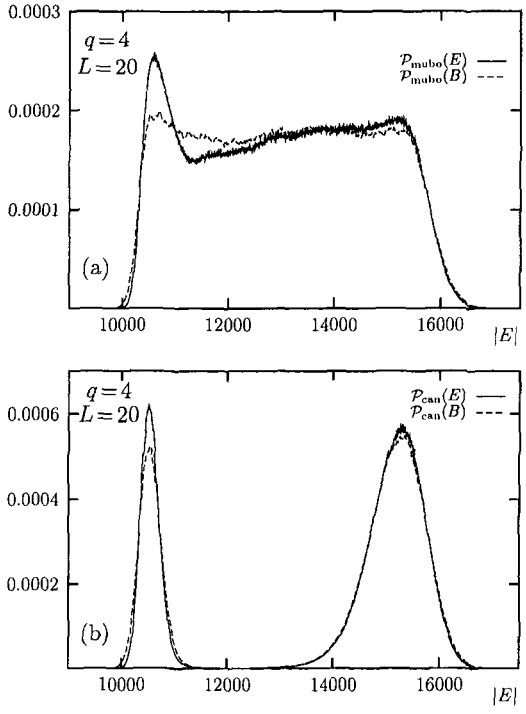

Fig. 1. (a) Bond and energy histograms in multibondic simulations for $q=4$, $L=20$, and $\beta=\beta_0=0.62857$. The bond histogram is plotted versus $(1+1/p)\,B$ with $p=\exp(\beta)-1$. In (b) these histograms are reweighted to the canonical ensemble, exhibiting in both observables the characteristic double-peak structure at a first-order phase transition.

the same simulation temperatures β_0. Below we report extensive simulations for $q=4$ on lattices of size $L=8$, 10, 12, 14, 16, 20, 24, and 30 (only multibondic), and for $q=5$ with $L=6$, 8, 10, 12, 14, 16, and 20. In addition we have studied for $q=3$ the two lattice sizes $L=10$ and 18 to get an overview of the general trend as a function of q. For all but the largest lattices we recorded in a time-series file 100 000 measurements of the energy E, the number of active bonds B, and the magnetization M, defined as

$$M=(q \max_k \{n_k\} - V)/(q-1) \tag{7}$$

where n_k denotes the number of spins with "orientation" $\sigma=k\in[1,q]$ in one configuration. Based on first rough estimates of autocorrelation times (see below) we performed N_{mubo} respectively N_{muca} sweeps between each of the measurements recorded in the time-series file, which were used for a later refined analysis of autocorrelation times. We furthermore stored *all* N_{mubo} (or N_{muca}) $\times 100000$ measurements of E, B, and M in energy, bond, and magnetization histograms. A more detailed overview of the simulation parameters is given in Table I.

3. AUTOCORRELATIONS

In order to evaluate the relative performance of the new multibondic and old multicanonical algorithm we shall focus in this paper on an analysis of their dynamical behavior as a function of the system size. We have, therefore, measured several autocorrelation times which will be always given in units of lattice sweeps.

A very intuitive definition employed in most previous multicanonical studies is the so-called flip (or in this context more properly diffusion) time, τ_e^{flip}, where one simply counts the average number of update sweeps that are needed to travel from $E<E_o$ to $E>E_d$ and back. More precisely, by comparison with the predictions of a canonical two-state model, this average number of update sweeps is identified with $4\tau_e^{\text{flip}}$. In our simulations the cuts E_o and E_d used in this definition were chosen to be identical to the reweighting boundaries given in Table I. Similarly, by replacing E with B or M, we can also define the flip times τ_b^{flip} or τ_m^{flip}. For accurate measurements it is important to test after *every* sweep if the system has passed one of these cuts. Performing the test only every N_{muca} or N_{mubo} sweep, we observed considerably larger values for τ^{flip}, simply because some of the cut crossings then can be missed. While this definition is very intuitive, its obvious drawback is the dependence on the adjustable cut parameters which introduces some arbitrariness.

A more objective measure of the performance is therefore the more formally defined autocorrelation time which in a *canonical* simulation would be derived for, e.g., the energy from the autocorrelation function

$$A_e(k) = \frac{\langle E_{i+k}; E_i \rangle}{\langle E_i; E_i \rangle} \tag{8}$$

where $\langle E_{i+k}; E_i \rangle \equiv \langle E_{i+k} E_i \rangle - \langle E_{i+k} \rangle \langle E_i \rangle$ is the time-displaced variance of the energy. For large time separations one expects an exponential decay

$$A_e(k) \to a_e \exp(-k/\tau_e^{\exp}) \tag{9}$$

where a_e is a constant and $\tau_e^{\exp}$ is the exponential autocorrelation time. As far as statistical errors of static quantities are concerned the so-called integrated autocorrelation time is more relevant. It is defined as

$$\tau_e^{\text{int}} = \tfrac{1}{2} + \sum_{k=1}^{N} A_e(k)(1 - k/N) \tag{10}$$

and can be shown to enter in the error estimate ε_e of mean values over N measurements, e.g., $\bar{E} = \sum_{k=1}^{N} E_k/N$, as

$$\varepsilon_e = \sqrt{\sigma_e^2/N}\,\sqrt{2\tau_e^{\text{int}}} \tag{11}$$

where σ_e^2 is the canonical variance, $\sigma_e^2 = \langle E^2 \rangle - \langle E \rangle^2$.

From (9) it is clear that for $k = f\tau_e^{\exp}$ with $f \approx 6...8$ the signal of $A_e(k)$ has dropped to about 1/1000 of its value at $k = 0$ (where it is by definition unity). For larger time separations the numerical estimates of $A_e(k)$ become quite noisy and the sum in (10) is therefore usually carried self-consistently only to $k_{\max} = f\tau_e^{\text{int}}$, with $f = 6...8$. Since in any meaningful simulation the number of measurements N is much larger than τ_e^{int}, the correction factor $(1 - k/N)$ in (10) can safely be neglected.

Also in multicanonical or multibondic simulation this would be precisely the way to proceed if multicanonical or multibondic expectation values would be of interest. Usually, however, one is only interested in canonical observables which can be recovered as ratios of multicanonical or multibondic expectation values, e.g.,

$$\langle E \rangle = \frac{\langle E w_e \rangle_{\text{muca}}}{\langle w_e \rangle_{\text{muca}}} = \frac{\langle E w_b \rangle_{\text{mubo}}}{\langle w_b \rangle_{\text{mubo}}} \tag{12}$$

where the expectation values $\langle \ldots \rangle_{\text{muca}}$ and $\langle \ldots \rangle_{\text{mubo}}$ are computed with Z_{muca} and Z_{mubo}, respectively, and $w_e \equiv e^{f_e}$ and $w_b \equiv e^{f_b}$ are the inverse reweighting factors. In analogy with (11) we therefore define an effective autocorrelation time τ_e^{eff} through

$$\varepsilon_e = \sqrt{\sigma_e^2/N}\,\sqrt{2\tau_e^{\text{eff}}} \tag{13}$$

where, as in (11), σ_e^2 is the canonical variance.

Technically we have now two possibilities to estimate ε_e and thus τ_e^{eff}. First, we can apply standard jack-knife blocking techniques[18] to directly estimate the statistical error of the estimator for $\langle Ew_e \rangle_{\text{muca}} / \langle w_e \rangle_{\text{muca}}$ or $\langle Ew_b \rangle_{\text{mubo}} / \langle w_b \rangle_{\text{mubo}}$ (which is simply the ratio of the mean values of Ew_e and w_e, or Ew_b and w_b). In the following this determination will be denoted by $\varepsilon_e^{\text{jack}}$ and τ_e^{jack}. The second, more elaborate method is to apply error propagation to (12). The result reads[19]

$$\varepsilon_e^2 = \langle E \rangle^2 \left[\frac{\langle Ew; Ew \rangle_{\text{mu}}}{\langle Ew \rangle_{\text{mu}}^2} \frac{2\tau_{Ew,Ew}^{\text{int}}}{N} + \frac{\langle w; w \rangle_{\text{mu}}}{\langle w \rangle_{\text{mu}}^2} \frac{2\tau_{w,w}^{\text{int}}}{N} - 2 \frac{\langle Ew; w \rangle_{\text{mu}}}{\langle Ew \rangle_{\text{mu}} \langle w \rangle_{\text{mu}}} \frac{2\tau_{Ew,w}^{\text{int}}}{N} \right] \tag{14}$$

where $\tau_{Ew,w}^{\text{int}}$, is the obvious generalization of the definition (10), w stands generically for w_e or w_b, and the subscript "mu" for "muca" or "mubo." The statistical error computed according to (14) will be denoted by $\varepsilon_e^{\text{eff}}$ and the resulting effective autocorrelation time by τ_e^{eff}. It should be emphasized that conceptually τ_e^{eff} and τ_e^{jack} are technically only alternative ways to estimate one and the same quantity. Any difference in the results must therefore be taken as an indication of statistical errors and systematic biases (which can be caused by the choice of the self-consistent cut-off in the determination of the integrated autocorrelation times and the number of blocks in the jack-knife procedure). The flip times τ_e^{flip}, on the other, are conceptually differently defined and can therefore not be expected to coincide with τ_e^{jack} or τ_e^{eff}.

4. RESULTS

Let us begin with the more extensively studied cases of $q = 4$ and 5. The measured autocorrelation times of E are collected in Tables II and IV. As an illustration how τ_e^{eff} is computed we show in Table III for $q = 4$ also the various variances, covariances and expectation values needed to evaluate (14). Since E and B are strongly correlated (recall Eq. (6)), the

Table II. Autocorrelation Times in Multicanonical and Multibondic Simulations for $q = 4$[a]

$D = 3$, $q = 4$, multicanonical							
L	$\tau^{\text{int}}_{E;E}$	$\tau^{\text{int}}_{Ew;Ew}$	$\tau^{\text{int}}_{w;w}$	$\tau^{\text{int}}_{Ew;w}$	τ^{eff}_{e}	τ^{jack}_{e}	τ^{flip}_{e}
8	51(5)	27(1)	13(1)	17(1)	61(3)	44	105(3)
10	99(13)	41(2)	25(1)	29(1)	121(6)	107	213(4)
12	167(20)	58(2)	44(1)	47(2)	228(11)	300	406(9)
14	264(20)	87(2)	69(2)	73(2)	412(19)	386	644(9)
16	375(19)	118(3)	102(2)	107(2)	591(26)	647	1063(19)
20	870(130)	196(5)	174(4)	179(4)	1365(49)	1835	2262(44)
24	1460(538)	274(15)	253(9)	259(12)	1932(595)	4353	5353(456)
$D = 3$, $q = 4$, multibondic							
L	$\tau^{\text{int}}_{E;E}$	$\tau^{\text{int}}_{Ew;Ew}$	$\tau^{\text{int}}_{w;w}$	$\tau^{\text{int}}_{Ew;w}$	τ^{eff}_{e}	τ^{jack}_{e}	τ^{flip}_{e}
8	71(5)	39(2)	9(1)	18(1)	77(5)	63	119(2)
10	95(10)	62(3)	38(2)	50(3)	107(8)	103	181(3)
12	148(12)	81(3)	53(2)	66(3)	189(34)	205	298(4)
14	229(24)	105(3)	74(2)	87(3)	316(21)	326	468(6)
16	303(27)	131(3)	100(4)	113(3)	488(65)	498	655(10)
20	584(41)	206(5)	166(4)	183(4)	940(58)	1009	1298(18)
24	1008(427)	280(10)	239(8)	256(11)	1607(473)	1471	2434(82)
30	2730(1293)	340(15)	334(13)	324(13)	3085(173)	4972	5429(238)
L	$\tau^{\text{int}}_{B;B}$	$\tau^{\text{int}}_{Bw;Bw}$	$\tau^{\text{int}}_{w;w}$	$\tau^{\text{int}}_{Bw;w}$	τ^{eff}_{b}	τ^{jack}_{b}	τ^{flip}_{b}
8	69(5)	40(2)	9(1)	18(1)	75(5)	62	106(2)
10	93(10)	62(3)	38(2)	50(3)	107(7)	102	177(3)
12	146(12)	81(3)	53(2)	66(3)	189(34)	204	286(4)
14	225(23)	104(3)	74(2)	87(3)	317(21)	327	451(6)
16	299(27)	131(3)	100(4)	113(3)	490(64)	498	649(10)
20	578(41)	206(5)	166(4)	183(4)	941(58)	1009	1281(18)
24	1005(427)	280(10)	239(8)	256(10)	1611(449)	1479	2418(83)
30	2723(1364)	340(15)	334(13)	324(13)	3081(172)	4978	5429(237)

[a] Error estimates are obtained with the jack-knife method on the basis of 100 blocks for $L = 8$–20, 40 (muca) resp. 50 (mubo) blocks for $L = 24$, and 40 blocks for $L = 30$.

various autocorrelation times of E and B are all indistinguishable within error bars. As an example we have included in Table II for the multibondic simulations also the autocorrelation times of B. We see that in most cases the corresponding numbers are, in fact, just identical, including the statistical error estimates. Also the autocorrelation times τ_m of the magnetization

Table III. Variances, Covariances, and Expectation Values of the Multibondic Simulations for $q=4$, Which Enter the Effective Error Estimate ϵ_e^{eff} [cf. Eq. (14)][a]

$D=3$, $q=4$, multibondic							
L	$\frac{\langle Ew;Ew\rangle}{\langle Ew\rangle^2}$	$\frac{\langle w;w\rangle}{\langle w\rangle^2}$	$\frac{\langle Ew;w\rangle}{\langle Ew\rangle\langle w\rangle}$	$\frac{\langle Ew\rangle}{\langle w\rangle V}$	σ_e^2	$\varepsilon_e^{\text{eff}}$	$\varepsilon_e^{\text{jack}}$
8	0.11208(70)	0.05993(28)	0.07032(46)	1.7495(42)	0.09751(67)	0.00462(13)	0.00417
10	0.2429(25)	0.15050(89)	0.1799(16)	1.7377(42)	0.08363(70)	0.00423(15)	0.00415
12	0.4471(52)	0.3418(26)	0.3759(37)	1.7339(40)	0.07731(71)	0.00383(45)	0.00398
14	0.6555(76)	0.5422(42)	0.5790(57)	1.7315(40)	0.07331(83)	0.00393(14)	0.00399
16	1.047(14)	0.9210(87)	0.961(11)	1.7447(38)	0.06988(92)	0.00369(25)	0.00373
20	1.561(22)	1.433(15)	1.468(18)	1.7395(38)	0.06992(94)	0.00363(13)	0.00376
24	2.175(71)	2.038(56)	2.077(62)	1.7654(68)	0.0615(22)	0.0070(11)	0.00673
30	2.555(91)	2.328(65)	2.381(73)	1.549(15)	0.0811(18)	0.01119(32)	0.01420

[a] σ_e^2 is the canonical variance of the energy. The number of jack-knife blocks for the computation of $\varepsilon_e^{\text{jack}}$ was 100 for $L=8-20$, 50 for $L=24$, and 40 for $L=30$.

Table IV. Autocorrelation Times in Multicanonical and Multibondic Simulations for $q=5$[a]

$D=3$, $q=5$, multicanonical							
L	$\tau_{E;E}^{\text{int}}$	$\tau_{Ew;Ew}^{\text{int}}$	$\tau_{w;w}^{\text{int}}$	$\tau_{Ew;w}^{\text{int}}$	τ_e^{eff}	τ_e^{jack}	τ_e^{flip}
6	32(4)	16(1)	7(1)	9(1)	38(3)	36	70(2)
8	74(6)	29(1)	19(1)	21(1)	104(4)	96	183(4)
10	149(10)	47(1)	36(1)	38(1)	234(7)	245	391(7)
12	268(19)	73(2)	60(1)	62(2)	467(13)	552	736(16)
14	738(55)	112(2)	151(4)	125(3)	1027(27)	1072	1140(11)
16	465(16)	113(2)	116(2)	111(2)	1467(62)	1621	1877(25)
20	1621(252)	271(9)	351(15)	304(19)	3095(919)	4056	3828(122)
$D=3$, $q=5$, multibondic							
L	$\tau_{E;E}^{\text{int}}$	$\tau_{Ew;Ew}^{\text{int}}$	$\tau_{w;w}^{\text{int}}$	$\tau_{Ew;w}^{\text{int}}$	τ_e^{eff}	τ_e^{jack}	τ_e^{flip}
6	60(3)	47(2)	24(1)	37(2)	64(4)	62	118(2)
8	127(9)	77(2)	47(1)	61(2)	156(8)	147	250(5)
10	220(16)	105(3)	69(2)	84(2)	324(16)	285	473(7)
12	381(21)	166(8)	115(3)	137(4)	630(120)	548	821(14)
14	535(22)	130(3)	168(4)	143(5)	1065(136)	1559	1300(21)
16	588(25)	208(5)	174(4)	188(4)	1636(67)	2057	1961(21)
20	2059(256)	237(7)	224(7)	224(7)	3149(120)	4109	4653(154)

[a] Error estimates are obtained with the jack-knife method on the basis of 100 blocks (40 blocks for $L=20$).

behave completely analogously and will therefore not be discussed separately. All error bars are estimated by means of the jack-knife method,[18] using usually 100 blocks.

We see that for small lattice sizes τ_e^{eff} and τ_e^{jack} are in good agreement, as they should be. For the largest lattice sizes our statistics are poorer and deviations are visible. We attribute this mainly to the relatively large statistical errors of τ_e^{jack}, which can be roughly estimated by varying the number of blocks used for computing $\varepsilon_e^{\text{jack}}$. The more intuitively defined flip times τ_e^{flip} are an upper bound on the more properly defined τ_e^{eff} or τ_e^{jack}.

Let us now turn to a discussion of the finite-size scaling behavior of the autocorrelation times. As already mentioned in the introduction, based on a random walk picture, one expects a power law,

$$\tau_e = aV^{\alpha} \tag{15}$$

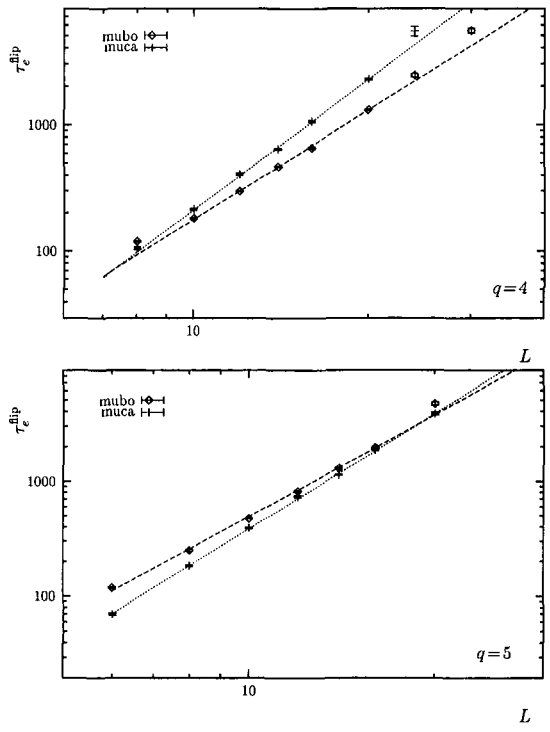

Fig. 2. Comparison of the flip times τ_e^{flip} of the energy in multibondic (mubo) and multicanonical (muca) simulations on a double logarithmic scale. The straight lines show fits according to the Ansatz (15). The resulting exponents α_e^{flip} are collected in Table V.

where $\mathcal{O}$ stands short for E or B. The argument goes as follows. For an idealized flat multicanonical (or multibondic) distribution, in each update step positive and negative energy changes ΔE (or bond-number changes ΔB) are equally likely. A lattice sweep consists of V spin updates. Viewing ΔE as the jumps of an uncorrelated one-dimensional random walk in energy we would therefore expect that after one sweep, on the average, the total energy change is $\sqrt{V}\,\Delta E$. Consequently, after V sweeps the energy would have changed, on the average, by an amount $\propto V\,\Delta E$, which is just the distance between the two peaks of the canonical energy distribution. In such an idealized picture, ignoring correlations between the jumps ΔE as well as boundary effects, one thus expects $\tau_{\mathcal{O}} \propto V^{\alpha}$ with $\alpha = 1$.

For the energy, the behavior of $\tau_{\mathcal{O}}^{\text{flip}}$ in multicanonical and multibondic simulations is compared in Fig. 2 for $q = 4$ and 5. For $\tau_{\mathcal{O}}^{\text{eff}}$ a similar comparison is shown in Fig. 3. In all cases we observe in the double-logarithmic plots the expected linear behavior. The straight lines are linear

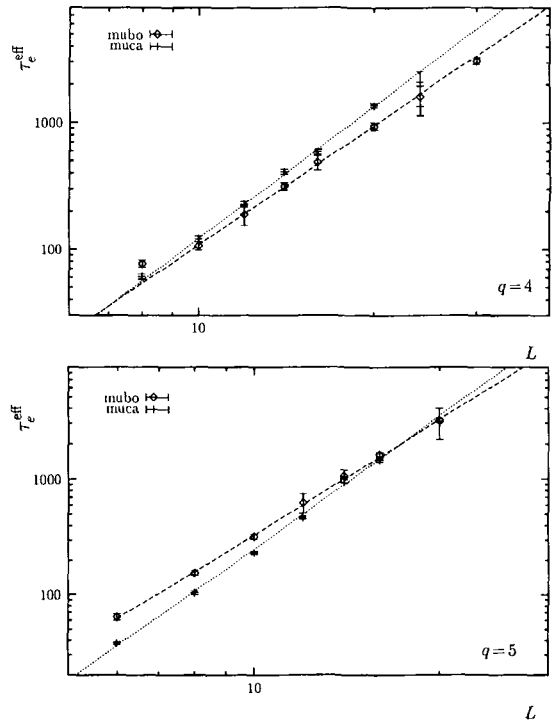

Fig. 3. Comparison of the effective autocorrelation times $\tau_{\mathcal{O}}^{\text{eff}}$ of the energy in multibondic (mubo) and multicanonical (muca) simulations on a double logarithmic scale. The straight lines show fits according to the Ansatz (15). The resulting exponents $\alpha_{\mathcal{O}}^{\text{eff}}$ are collected in Table V.

Table V. Dynamical Exponents α Obtained from Fits of τ_e^{eff}, τ_e^{jack}, and τ_e^{flip} According to the Ansatz (15) in Multibondic (mubo) and Multicanonical (muca) Simulations of the 3D q-State Potts Model

	$q=4$		$q=5$	
	mubo	muca	mubo	muca
α_e^{eff}	1.04(5)	1.15(3)	1.09(2)	1.26(2)
α_e^{jack}	1.02(8)	1.37(9)	1.21(8)	1.33(7)
α_e^{flip}	0.96(1)	1.14(2)	0.98(1)	1.11(1)

least-squares fits which yield the values of α collected in Table V. For the multibondic algorithm we obtain as in two dimensions values around $\alpha \approx 1.0$, while for the multicanonical simulations we find also in three dimensions a larger value of $\alpha \approx 1.2$ (which, however, is little smaller than in two dimensions). Since the computational effort is roughly the same for the two algorithms we can therefore conclude that, asymptotically for large system sizes, also in three dimensions the multibondic algorithm is always favorable.

The actual autocorrelation times for a given lattice size depend, of course, also on the prefactor a in (15). This is the reason why at the very strong first-order phase transition for $q=5$ the multicanonical τ's in Figs. 2 and 3 are smaller than the multibondic τ's for small lattice sizes. Here the crossover between the two algorithms happens around $L=20$. At the weaker first-order transition for $q=4$, however, the autocorrelations of the multibondic algorithm are smaller already for lattice sizes as small as $L=10$. Qualitatively the same effect was also observed in two dimensions.[12]

This behavior suggests that for $q=3$ the multibondic algorithm should be superior for all reasonable system sizes. Our data for $L=10$ and 18 clearly confirm this claim. The results of the multicanonical simulations are $\tau_e^{\text{jack}}=44.8(1.2)$ and 234.1(5.1) for $L=10$ and 18, and in the multibondic simulations we obtain $\tau_e^{\text{jack}}=25.03(56)$ and 77.2(2.8) for $L=10$ and 18. Already for the modest size $L=10$ the multibondic algorithm is thus two times faster than standard multicanonical simulations, and for $L=18$ we find already an improvement factor of about three.

In Fig. 4 we finally show for the multibondic algorithm a comparison of the three autocorrelation times. We see that τ_e^{eff} and τ_e^{jack} are almost indistinguishable, as they should be. The flip times τ_e^{flip}, on the other hand,

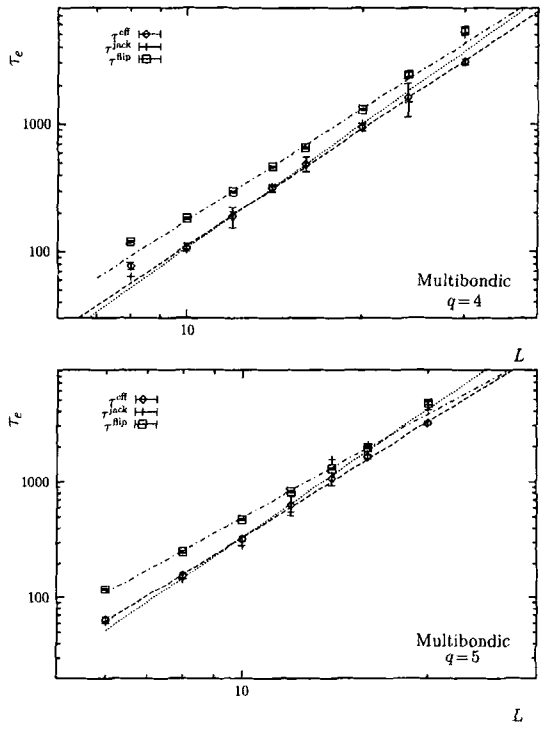

Fig. 4. Comparison of the autocorrelation times τ_e^{eff}, τ_e^{jack}, and τ_e^{flip} of the energy in multibondic simulations on a double logarithmic scale. The straight lines show fits according to the Ansatz (15). The resulting exponents α_e^{eff}, α_e^{jack}, and α_e^{flip} are collected in Table V.

are larger by roughly a constant factor. The constant factor is also reflected in Table V by the fitted exponents α, which are roughly the same for all three definitions of τ_e. Since this is the case for both, $q=4$ and $q=5$, and was also observed for the two-dimensional model, this seems to be a generic feature of this heuristic definition.

Due to the improved performance of multicanonical and in particular multibondic simulations we have been able to perform detailed finite-size scaling analyses of the first-order phase transitions in the three-dimensional q-state Potts model with $q \geqslant 3$. This allowed us to determine high-precision estimates of the transition temperature β_t from fits to the power-law scaling of the locations of the specific-heat maxima and energetic Binder-parameter minima, and to confirm that the refined pseudo-transition temperatures defined in ref. 20 exhibit only exponentially small finite-size corrections. Another important quantity characterizing the strength of a first-order phase transition is the interface tension σ_{od} between the ordered and

disordered phase. To estimate σ_{od} we used the histogram method[21] which is based on the fundamental relation $\mathscr{P}_{\text{can}}^{\min}/\mathscr{P}_{\text{can}}^{\max} \propto \exp(-2\sigma_{od}L^{d-1})$ discussed in the introduction. Since it is precisely this property of first-order phase transitions which leads in canonical simulations to supercritical slowing down with autocorrelation times that are exponentially large in the system size, it is essential to use multicanonical or multibondic simulations to exploit this relation. In fact, our results of $2\sigma_{od} \approx 0.02$ for $q=4$ and $2\sigma_{od} \approx 0.05$ for $q=5$ imply that the largest system sizes considered in this study have extremely long canonical autocorrelation times of the order of 10^7–10^8. In addition we also investigated the very peculiar finite-size scaling behavior of the magnetic Binder cumulant at a first-order phase transition[22] and obtained for the first time clear evidence for multiplicative logarithmic corrections in the scaling behavior. A detailed discussion of our quite elaborate finite-size scaling analysis would be beyond the scope of this article and will be reported separately.

5. CONCLUSIONS

We performed a very careful comparison of the dynamical behavior of the multibondic and the multicanonical algorithm at the first-order phase transition of the three-dimensional q-state Potts model with $q=4$ and 5. Our results show that the autocorrelation times in multibondic simulations scale with the system size according to $\tau \propto V^{\alpha}$, with $\alpha \approx 1$, in very good agreement with the prediction of a simple random walk argument. For multicanonical simulations we obtained an estimate of $\alpha \approx 1.2$. This implies that, asymptotically for large system sizes, multibondic simulations are always favorable.

For smaller systems the multibondic algorithm is found to be increasingly more efficient than the multicanonical as q decreases for the same lattice size, such that in the particular case of any high-precision studies of the first-order phase transition of the three-dimensional 3-state Potts model the multibondic algorithm is the ideal tool.

ACKNOWLEDGMENTS

MSC acknowledges a Fulbright fellowship, WJ thanks the Deutsche Forschungsgemeinschaft for a Heisenberg fellowship, and SK acknowledges a fellowship by the Graduiertenkolleg "Physik and Chemie supramolekularer Systeme." This work was supported by computer grants hkf001 of HLRZ Jülich and bvpf03 of Norddeutscher Vektorrechnerverbund (NVV) Berlin-Hannover-Kiel.

REFERENCES

1. K. Binder, in *Phase Transitions and Critical Phenomena*, Vol. 5b, C. Domb and M. S. Green, eds. (Academic Press, New York, 1976), p. 1; and in *Monte Carlo Methods in Statistical Physics*, K. Binder, ed. (Springer, Berlin, 1979), p. 1.
2. A. D. Sokal, *Monte Carlo Methods in Statistical Mechanics: Foundations and New Algorithms*, Cours de Troisième Cycle de la Physique en Suisse Romande, Lausanne, 1989; and Bosonic Algorithms, in *Quantum Fields on the Computer*, M. Creutz, ed. (World Scientific, Singapore, 1992), p. 211.
3. W. Janke, Monte Carlo Simulations of Spin Systems, in *Computational Physics: Selected Methods—Simple Exercises—Serious Applications*, K. H. Hoffmann and M. Schreiber, eds. (Springer, Berlin, 1996), p. 10.
4. W. Janke, Nonlocal Monte Carlo Algorithms for Statistical Physics Applications, Mainz preprint (April 1997), to appear in *Monte Carlo Methods*, Proceedings of the IMACS Workshop, Brussels, April 1997.
5. H. J. Herrmann, W. Janke, and F. Karsch (eds.), *Dynamics of First Order Phase Transitions* (World Scientific, Singapore, 1992); K. Binder, *Rep. Prog. Phys.* **50**:783 (1987); J. D. Gunton, M. S. Miguel, and P. S. Sahni, in *Phase Transitions and Critical Phenomena*, Vol. 8, C. Domb and J. L. Lebowitz, eds. (Academic Press, New York, 1983), p. 269.
6. A. Billoire, *Nucl. Phys. B (Proc. Suppl.)* **42**:21 (1995); W. Janke, in *Computer Simulations in Condensed Matter Physics VII*, D. P. Landau, K. K. Mon, and H. B. Schüttler, eds. (Springer, Berlin, 1994), p. 29.
7. B. A. Berg and T. Neuhaus, *Phys. Lett. B* **267**:249 (1991).
8. B. A. Berg and T. Neuhaus, *Phys. Rev. Lett.* **68**:9 (1992).
9. For reviews and a discussion of related approaches, see B. A. Berg, in *Dynamics of First Order Phase Transitions* [ref. 5], p. 311; and in *Multiscale Phenomena and Their Simulation*, F. Karsch, B. Monien, and H. Satz, eds. (World Scientific, Singapore, 1997), p. 137.
10. W. Janke, in *Physics Computing '92*, R. A. de Groot and J. Nadrchal, eds. (World Scientific, Singapore, 1993), p. 351.
11. W. Janke, B. A. Berg, and M. Katoot, *Nucl. Phys. B* **382**:649 (1992).
12. W. Janke and S. Kappler, *Phys. Rev. Lett.* **74**:212 (1995).
13. R. B. Potts, *Proc. Camb. Phil. Soc.* **48**:106 (1952).
14. F.Y. Wu, *Rev. Mod. Phys.* **54**:235 (1982); **55**:315(E) (1983).
15. W. Janke and R. Villanova, *Nucl. Phys. B* **489**:679 (1997); and references to earlier work therein.
16. P. W. Kasteleyn and C. M. Fortuin, *J. Phys. Soc. Japan* **26**(Suppl.):11 (1969); C. M. Fortuin and P. W. Kasteleyn, *Physica* **57**:536 (1972); C. M. Fortuin, *Physica* **58**:393 (1972); **59**:545 (1972).
17. R. H. Swendsen and J.-S. Wang, *Phys. Rev. Lett.* **58**:86 (1987).
18. R. G. Miller, *Biometrika* **61**:1 (1974); B. Efron, *The Jackknife, the Bootstrap and Other Resampling Plans* (SIAM, Philadelphia, 1982).
19. W. Janke and T. Sauer, *J. Stat. Phys.* **78**:759 (1995).
20. C. Borgs and W. Janke, *Phys. Rev. Lett.* **68**:1738 (1992); W. Janke, *Phys. Rev. B* **47**:14757 (1993).
21. K. Binder, *Phys. Rev. A* **25**:1699 (1982).
22. K. Vollmayr, J. D. Reger, M. Scheucher, and K. Binder, *Z. Phys. B* **91**:113 (1993).